CALIBRATION AND VALIDATION OF AN ALGORITHM FOR REMOTE SENSING OF TURBIDITY OVER LA PLATA RIVER ESTUARY, ARGENTINA

Ana I. Dogliotti[1,2], Kevin Ruddick[1], Bouchra Nechad[1], Carlos Lasta[3], Alejandra Mercado[3], Constanza Hozbor[3], Raúl Guerrero[3], Gabriela Riviello López[4], and Mariana Abelando[4]

1. Management Unit of the North Sea Mathematical Models (MUMM), Royal Belgian Institute of Natural Sciences (RBINS), 100 Gulledelle, 1200 Brussels, Belgium; ana.dogliotti(at)mumm.ac.be, adogliotti(at)iafe.uba.ar
2. Instituto de Astronomía y Física del Espacio (IAFE), CONICET/UBA, Buenos Aires, Argentina
3. Instituto Nacional de Investigación y Desarrollo Pesquero (INIDEP), Mar del Plata, Argentina
4. Prefectura Naval Argentina (PNA), Buenos Aires, Argentina

ABSTRACT

The La Plata River, located at 35°S on the Atlantic coast, is one of the largest waterways of South America. It carries a large amount of suspended particulate and dissolved organic matter, and is considered among the most turbid waters of the world. Very high values of total suspended matter have been reported in this region, with mean values ranging from 100 to 300 g m^{-3} and extreme concentrations up to 400 g m^{-3}. Satellite sensors have shown to be the best tools available to map river plumes and to study their influence on the adjacent ocean. However, global algorithms for remotely estimating sediment concentration are not currently available. Moreover, such high sediment loads represent a challenge to atmospheric correction algorithms which usually rely on the assumption of zero water-leaving reflectance in the near infrared or short wave infrared part of the spectrum (black pixel assumption). In the extremely turbid waters of La Plata Estuary such assumptions are not valid. A two band algorithm to estimate turbidity using near infrared and the short wave infrared bands (858 nm and 1240 nm) of the MODIS-Aqua sensor is presented. The model is calibrated using *in situ* reflectance and turbidity measurements from turbid waters of the Southern North Sea and Scheldt River (Belgium) and then applied to MODIS imagery of La Plata River estuary (Argentina). A good correlation was found between modelled and *in situ* turbidity values when the algorithm was applied to concurrent MODIS imagery. Moreover, satellite-derived turbidity maps show a spatial distribution of sediment consistent with patterns and characteristic features of the estuary.

INTRODUCTION

La Plata River is an extensive (~3.5 · 10^4 km^2) and shallow (<20 m) estuary located in the eastern coast of South America at ~35°S (Figure 1). It drains the second largest basin of South America, after the Amazon River, carrying high amounts of nutrients, suspended particulate and dissolved organic matter to the adjacent shelf waters. Considered one of the most turbid waters in the world, La Plata River is characterised by the presence of a turbidity front associated with the transition between the freshwater outflow and the brackish water, which constitutes a dynamical boundary between the upper and lower part of the estuary (1). The mean distribution of the turbidity front in La Plata River is strongly related to the bottom topography (2). At the southern coast, in the Samborombón Bay, its mode position coincides with the 5 m depth contour, and to the north it follows the Barra del Indio shoal, a shallow bar that runs along a line from Punta Piedras to Montevideo (Figure 1).

La Plata River estuary is an area of high economical and ecological importance. In particular, the region associated to the turbidity front is an area of enhanced plankton concentration (3) and is the primary spawning and nursery area for many estuarine species that are commercially exploited and support coastal fisheries of Argentina and Uruguay (4,5,6,7,8,9). Samborombón Bay, located

to the south of the river mouth, is one of the most important wetlands of Argentina and is home to a number of species of turtles, crabs and migratory birds (10,11).
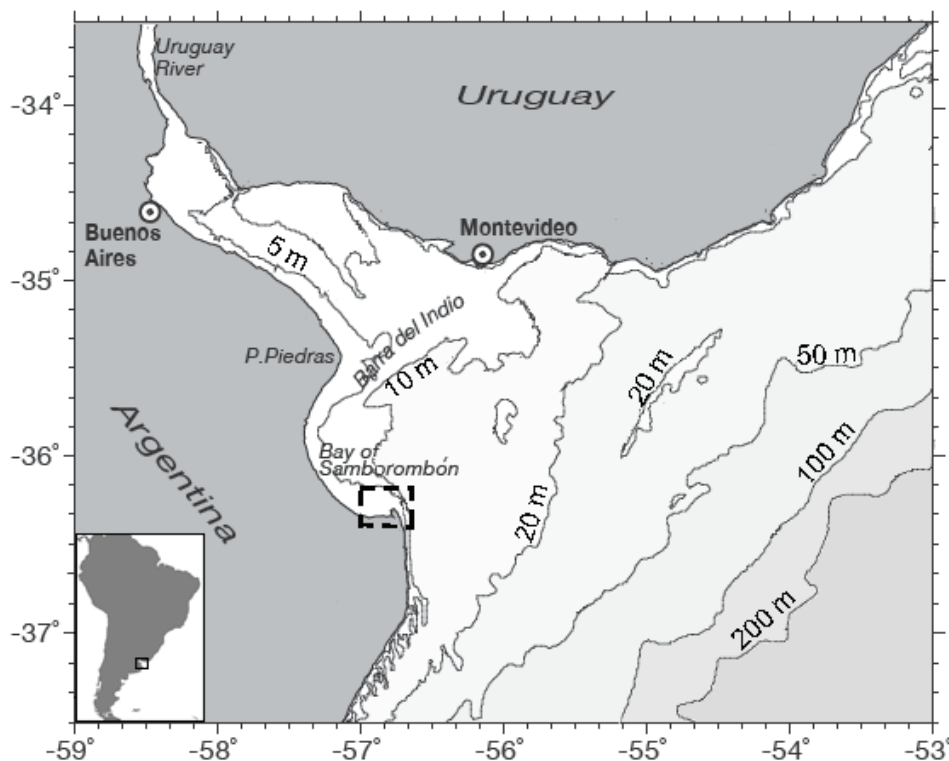
Figure 1: Location and bathymetry of the study area, La Plata River estuary. Dashed rectangle indicates the region where in situ measurements have been collected.

Satellite sensors have shown to be useful tools to map river plumes and to study their influence on the adjacent ocean (12,13,14). Moreover, they provide good spatial and temporal coverage of the whole La Plata estuary, but the accurate retrieval of in water constituents is hindered by the performance of the atmospheric algorithms. In these highly turbid waters, the standard atmospheric correction algorithms are known to fail (15,16,17,18,19,20), thus an alternative way for deriving in water constituents seems an appealing solution. Previous work using satellite imagery in this region has focused mainly on determining the frontal location and its spatio-temporal distribution (2), but only one has attempted the quantitative retrieval of sediment concentration (21).

The objective of the present study is to use MODIS-Aqua observations of Rayleigh-corrected reflectance in the near infrared (NIR) and short wave near infrared (SWIR) bands to estimate turbidity in the Samborombón Bay, a region influenced by La Plata River discharge and sediment resuspension. First, a turbidity retrieval algorithm is presented. Then, the model is calibrated using *in situ* reflectance and turbidity data from turbid waters of the Southern North Sea and Scheldt River. And finally, turbidity is computed from MODIS-Aqua Rayleigh-corrected reflectance over the Samborombón Bay and compared to concurrent turbidity measurements.

METHODS

Turbidity model

Turbidity provides a measure of water clarity and is measured via the scattered light resulting from the interaction between a beam of light and suspended particles in a water sample. In the present study we follow the International Organization for Standarization (ISO 7027) definition and specifications of the method, i.e. measurement of the side-scattering of a monochromatic infrared light at 860nm. Thus, it is defined as the reduction of transparency of a liquid caused by the presence of non dissolved matter (22).

The theoretical basis for the algorithm developed in this study is based on the one-band Turbidity (*T*) and Total Suspended Matter (*TSM*) algorithms described in (23,24), respectively. For brevity only the turbidity algorithm will be described, but in a similar way the *TSM* algorithm can also be derived. The algorithm relates turbidity (*T*) to water reflectance, ρ_w, through

$$\rho_w = \frac{T}{A_T + T/C} \qquad (1)$$

where A_T and C are two wavelength-dependent calibration coefficients. The parameter *C* was calibrated using "standard" inherent optical properties, i.e. using average coefficients and typical values for coastal waters found in the literature; for more details and the tabulated values see (24). The A_T factor was obtained by a non linear least-square regression analysis using *in situ* measurements of *T* and ρ_w from the Southern North Sea (23) and is related theoretically to inherent optical properties as shown later. Thus, applying this model at two different wavelengths the following relation between turbidity and the reflectance difference between band 1 and 2 ($\Delta\rho_w^{1,2}$) is proposed:

$$\Delta\rho_w^{1,2} = \frac{T}{A_{T1} + T/C_1} - \frac{T}{A_{T2} + T/C_2} \qquad (2)$$

When applied to remotely sensed data, the use of a band difference of Rayleigh-corrected reflectance at two relatively close bands avoids the use of an aerosol correction algorithm by assuming spectrally "white" aerosols. For the present algorithm the MODIS 858 and 1240 nm bands were chosen. Analysis of MODIS imagery over La Plata River estuary showed that the MODIS 869 nm ocean band usually saturates in this region, preventing its use in the turbidity model. Consequently, the high resolution (250 m) land band at 858 nm is used instead.

The calibration coefficients A_T and *C* have been previously tabulated only between 600-885 nm (23,24). Therefore to apply this algorithm to the short wave infrared band, i.e. 1240 nm band, the calibration had to be extended. The A_T factor is given theoretically by

$$A_T = \frac{a_{np}}{\gamma b_{bpT}^*} \qquad (3)$$

where a_{np} is the non-particulate absorption coefficient, γ is a factor relating reflectance to inherent optical properties and b_{bpT}^* is the turbidity-specific particulate backscatter coefficient, see (23) for details. Comparison between the shape of the spectrum of A_T established using regression analysis of reflectance and turbidity data and the pure water absorption spectrum (both normalized to their values at 780 nm) - Figure 3 of (23) - suggest that values established for the range 700-900 nm can be extrapolated to the SWIR range by assuming spectrally invariant γ and $a_{np} \approx a_w$, where a_w is the pure water absorption coefficient. Thus:

$$A_T(\lambda) = A_T(858\,\text{nm}) \cdot \frac{a_w(\lambda)}{a_w(858\,\text{nm})} \cdot \frac{b_{bpT}^*(858\,\text{nm})}{b_{bpT}^*(\lambda)} \qquad (4)$$

Studies of the spectral variation of particulate backscatter (25) suggest that the turbidity-specific particulate backscatter coefficient can be assumed to follow a power law formulated as:

$$b_{bpT}^*(\lambda) = b_{bpT}^*(858\,\text{nm}) \cdot \left(\frac{\lambda}{858\,\text{nm}}\right)^{-n} \qquad (5)$$

where the exponent *n* is a parameter describing the spectral dependency of particle backscattering. Combining equations 4 and 5 gives:

$$A_T(\lambda) = A_T(858\,\text{nm}) \cdot \frac{a_w(\lambda)}{a_w(858\,\text{nm})} \cdot \left(\frac{\lambda}{858\,\text{nm}}\right)^{n} \qquad (6)$$

Thus, taking values for $a_w(\lambda)$ from (26), using $n = 0.4$ as a mean value found in measurements of the particulate scattering coefficient (27), and assuming spectrally constant scattering to backscattering ratio, A_T at 1240 nm can be derived (see Results). The C coefficient was calculated as in (24) from

$$C = \gamma \frac{b_{bpT}^*}{a_{np} + b_{bpT}^*} \qquad (7)$$

The "standard" inherent optical properties were extrapolated to the SWIR region assuming a spectrally constant particle scattering to backscattering ratio.

The resulting model for retrieving T by inversion of Eq. 2 is a quadratic equation that yields two possible solutions; one represents the low T range, while the other is the higher level (Figure 2). Details regarding the inversion of the model are given in Appendix A.
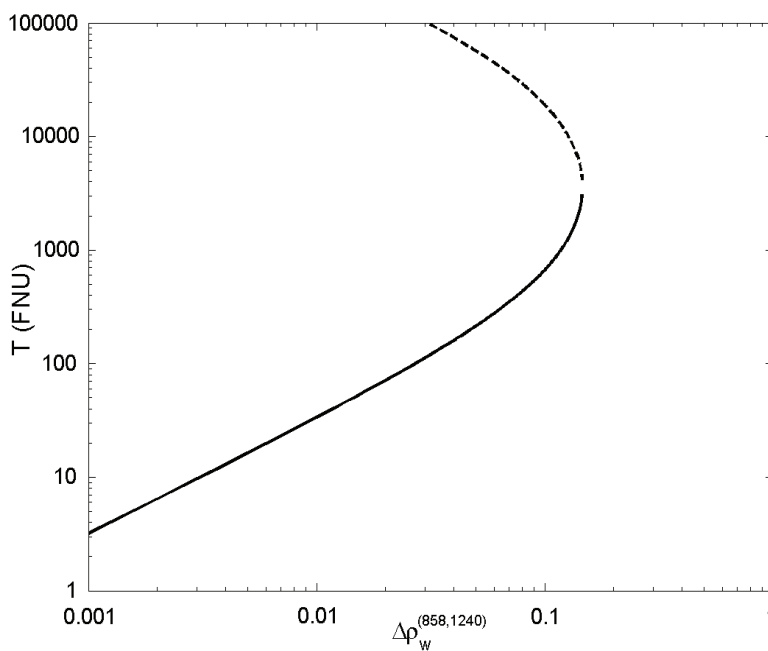
Figure 2: Two-band model relating the reflectance difference between 858 and 1240 nm and turbidity using equation (1) in the present study. The solid and dashed lines are the two possible solutions of the quadratic equation.

In situ data

Two data sets of concurrent *in situ* measurements of reflectance and turbidity were used to recalibrate the one-band turbidity algorithm in the NIR (Table 1). One data set was collected in the Southern North Sea (SNS), from 2007 to 2010, during 12 cruises onboard the Belgica research vessel. This region is a relatively shallow area (<50 m) subject to strong vertical mixing from strong winds and tidal currents (28). Sediment resuspension causes relatively high *TSM* concentrations (~1 - 200 g m^{-3}). The second data set corresponds to measurements performed from a fixed pontoon (51°14'N - 4°23'E) located near the city of Antwerp (Belgium) in the Scheldt River (SR). Measurements were made during two days, from 10:00 to 15:00 local time, in July 15 and October 26, 2010. The Scheldt is a relatively turbid estuary with *TSM* values that can reach up to 400 g m^{-3} and a strong tidal and seasonal variation (29).

Above-water marine reflectance measurements were collected with a set of three TriOS-RAMSES hyperspectral spectroradiometers with a sampling interval of approximately 3.3 nm and an effective spectral resolution of about 10 nm covering the spectral range 400-900 nm and following the protocol described in (17). The same quality control was applied to the data, except for the homogenous sky condition which was relaxed since it was not always met during the SR measurements.

Turbidity was measured using a portable HACH 2100P ISO turbidimeter as in (23). The instrument records turbidity between 0 and 1000 FNU (Formazin Nephelometric Units), with a resolution of 0.01 FNU. The instrument measures turbidity via the ratio of 90°-scattered light to forward-transmitted light of monochromatic infrared (860 nm) light. The turbidimeter was calibrated in April 2007 using a set of Stabilized Formazin Turbidity Standards (STABLCAL) with turbidities of <0.1, 20, 100 and 800 FNU, prepared according to the instructions of the manufacturer. Turbidities of these standards were also recorded after each sampling day to check the instrument stability.

A third data set consisted of *in situ* turbidity measurements performed in the southern region of Samborombón Bay (Argentina) (Figure 1). They were used to test the turbidity algorithm using co-incident satellite-retrieved reflectances. Turbidity measurements were performed on surface samples obtained in two cruises on board Guardacostas 122 "LAGO MASCARDI" vessel in December 20, 2010 and March 21, 2011, using the Multi Parameter Water Quality Monitoring System HORIBA, model U-22XD (Table 1). This equipment measures turbidity in the range 0-800 FNU, with a resolution of 0.1 FNU. The measurement method is similar to the HACH sensor (transmission-scattering), but the scattered near infrared light is measured at an angle of 60° instead of 90° relative to the light source.

Table 1: Summary of the data sets used in the present study: Southern North Sea (SNS), Scheldt River (SR) and Samborombón Bay (SB).

Region	Period	Turbidity range (FNU)	Number of stations
SNS	2007-2010	10.7-88.4	29
SR	15 Jul; 26 Oct, 2010	52.3-255.3	23
SB	20 Dec 2010; 21 Mar 2011	6-270	19

Satellite data

Level 1A MODIS-Aqua images from the sampling dates over Samborombón Bay (December 20, 2010 and March 21, 2011) were obtained from the NASA Ocean Color website and processed to level 2 to obtain Rayleigh-corrected reflectance at all bands i, ρ_{rc}^i, using SeaDAS 6.2. Clouds were masked using the Rayleigh-corrected reflectance at 2130 nm band and a threshold of 0.018. The median of the Rayleigh-corrected reflectance values of a 3×3 pixel box centred at the location of the sample sites was extracted and used as input to test the turbidity algorithm. The time difference between the field measurements and the satellite overpass varied between 5 minutes to 4 hours.

RESULTS

Model calibration

The algorithm described in the present study was re-calibrated as in (23), but using a different data set that included higher T values. The A_T coefficient at 858 nm was determined by non-linear regression analysis of *in situ* water reflectance and turbidity measurements performed in the Southern North Sea (SNS) and the Scheldt River (SR); only values higher than 10 FNU were used. Figure 3 shows the fitted curve (solid line) and the calibration data set used in the present study for the water reflectance at MODIS 858 nm band (solid symbols). Also the previous fit (dashed line) and the whole SNS data base (round solid and open symbols) are shown for comparison. The previous and new calibration coefficients and their standard error are shown in Table 2.
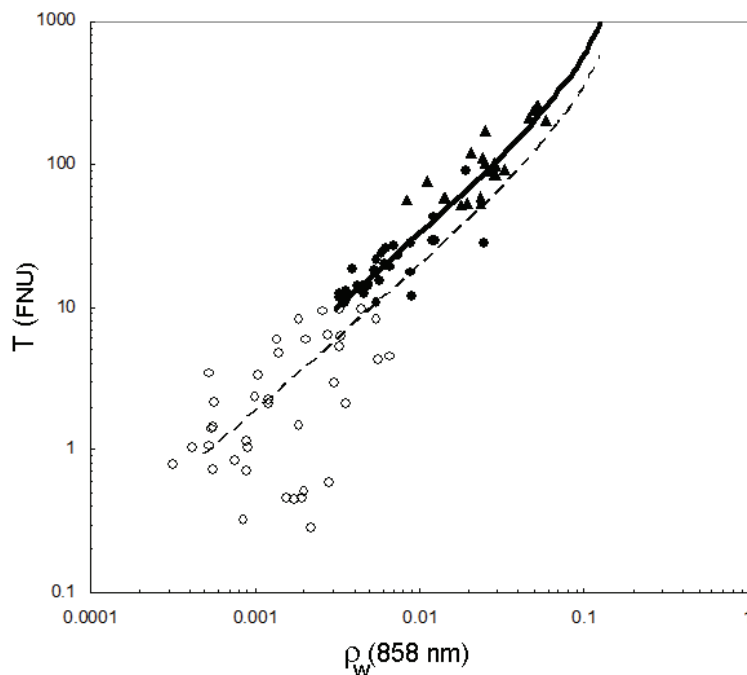
Figure 3: Best fitting curve for equation (1) in the present study (bold line) derived by regression analysis of seaborne reflectance at 858 nm and turbidity measurements with T>10 FNU in the SNS (solid round symbols) and Scheldt River (solid triangles). Previous best fitting curve obtained using the whole SNS data set (open and solid round symbols) is also shown (dashed line).

A good performance of the curve fitting was found with a R^2 of 87.6% (calculated using Eq. 17 in (24)). The new derived A_T was higher than previously determined in (23), referred to as BN09, and a recently updated version using only SNS data from 2007-2010 cruises (BN11), because it is now based only on high water reflectance measurements where there is lower relative measurement uncertainty.

Table 2: Calibration coefficients C and A_T (FNU) for the MODIS bands used in the previous work (BN09), a recently updated version (BN11) and the one obtained with the new calibration (NEW). ΔA_T is the standard error and n the number of data used in the non-liner regression for the NIR.

λ (nm)	C	A_T (BN09) $\pm$ ΔA_T	A_T (BN11) $\pm \Delta A_T$	A_T (NEW) $\pm \Delta A_T$
858	$21.1 \cdot 10^{-2}$	2042.9 ± 175.1 (n=26)	1845.8 ± 222.6 (n=68)	3078.9 ± 178.0 (n=52)
1240	$21.6 \cdot 10^{-2}$	-	-	94117.2 ± 5441.2

Validation of turbidity algorithm

The proposed algorithm to estimate turbidity was tested and evaluated using the MODIS satellite-retrieved Rayleigh-corrected reflectance values for the days of the cruises in the Samborombón Bay region (dashed rectangle in Figure 1). Figure 4 shows the location of the sampled stations over the corresponding turbidity maps derived from the model using MODIS 858 and 1240 nm bands.

To evaluate the algorithm performance, the log_{10} root-mean square (log_{10}-RMS) of the log_{10}-difference error between measured and modelled turbidity at each station was calculated. Also, the relative error (RE) and absolute percentage difference (APD) between the measured and modelled values was calculated to estimate bias and uncertainty, respectively. The scatter plots and statistics of the analysis for the two sampling dates in Samborombón Bay are shown in Figure 5 and Table 3, respectively.
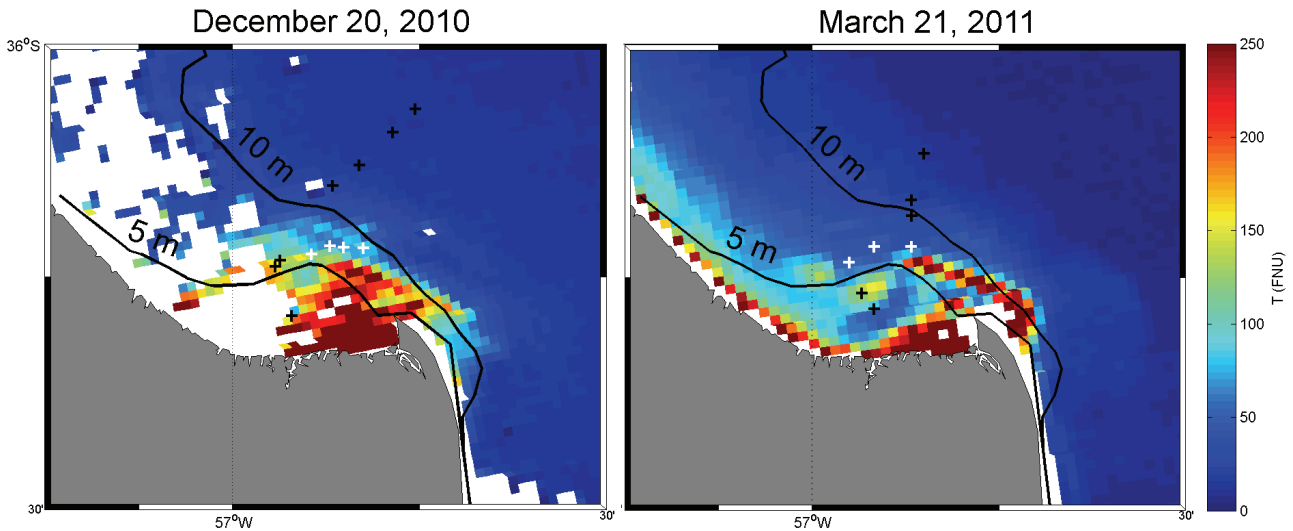
Figure 4: Turbidity maps from MODIS Rayleigh-corrected band-difference reflectance at 858 and 1240 nm on December 20, 2010 at 17:50 UTC (left) and on March 21, 2011 at 17:35 UTC (right) over Samborombón Bay. Location of the sampled stations (+) and the 5 and 10 metre contours are indicated on the images (black lines). Regions with clouds are in white.
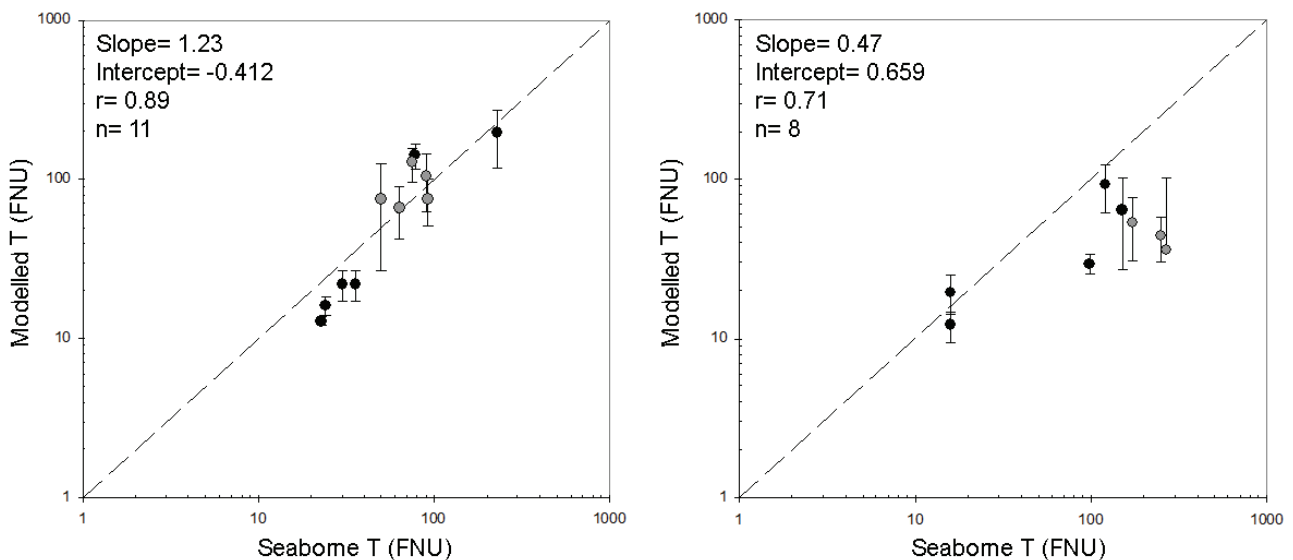
Figure 5: Scatter plots of seaborne and modelled turbidity using MODIS-Aqua Rayleigh-corrected reflectance in Samborombón Bay in December 20, 2010 (left) and March 21, 2011 (right). Error bars are the standard deviation of a 5×5 pixel window centred at the sampled site. The grey symbols correspond to stations indicated in white in Figure 4. The dashed curve shows the 1:1 line.

In general, the band-difference algorithm performed reasonably well. A better agreement was found for the first cruise compared to the second (Figure 5 and Table 3). The first showed a higher correlation (0.89), a slope closer to 1 (1.23) and lower Log_{10}-RMS error (0.1914).

When considering the performance of the algorithm, it is important to assess the effect of spatial and temporal mismatch between *in situ* and remote sensing data. The relative error showed no significant correlation with the time difference between the sampling and the satellite overpass ($p>0.1$) (Figure 6a). However, part of the differences found between measured and modelled values could be related to the high spatial variability of the sediment distribution. Stations located following a high turbidity feature with high *T*, between the 5 and 10 m contour lines (Figure 4), showed the highest spatial variability as indicate the large standard deviations calculated from a 5×5 pixel window centred at the sampled site (grey symbols and stations in Figure 5 and 4, respectively). Moreover, the analysis of one year of Turbidity maps obtained using the proposed algorithm

(Jan-Dec 2009, *N*=117) showed that the region between 5-10 m depth presents a high variability, as shown by the high standard deviation values found (~100 FNU) (Figure 6b).

Table 3: Algorithm statistics for the turbidity model applied to the two cruises. APD is the mean absolute percentage difference and log$_{10}$-RSM is the root-mean square of the log transformed data.

Date	APD(%)	Log$_{10}$RMS	Slope	Intercept	R^2	N
20 Dec 2010	42.9	0.1914	1.23	-0.414	0.79	11
21 Mar 2011	48.4	0.4947	0.48	0.659	0.51	8
All	45.2	0.3525	0.63	0.511	0.43	19
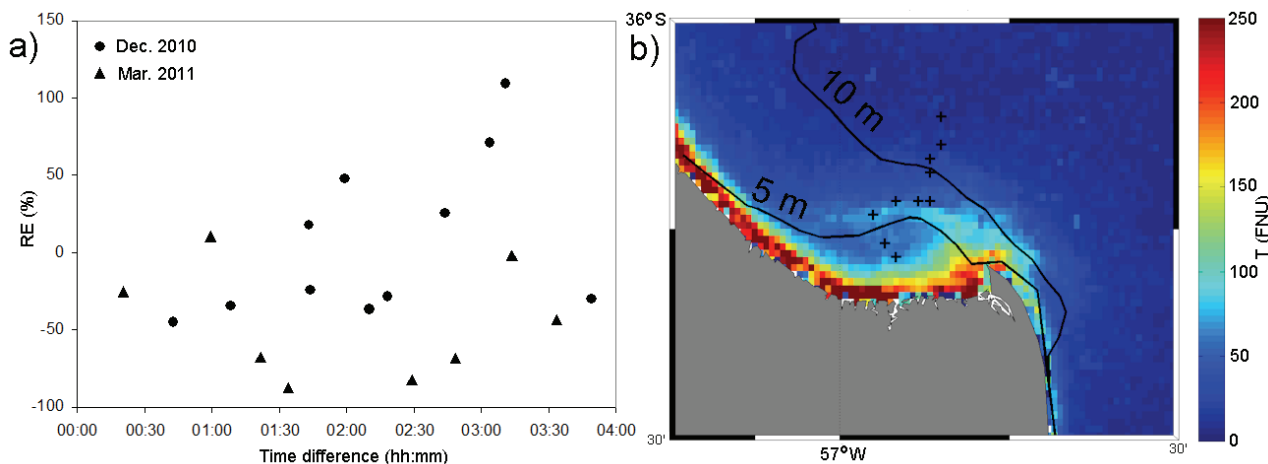
Figure 6: a) Relative percent error as a function of time difference between in situ measurements and satellite overpass for the two cruise dates; b) Standard deviation map of turbidity obtained from daily MODIS-Aqua images for the period Jan-Dec 2009 (N=117). The 5 and 10 metre contour lines are indicated (black lines).

The highly turbid waters of La Plata River can be clearly seen in the MODIS quasi-true-colour images corresponding to the sampling dates by their brown colour (Figure 7). The derived turbidity maps using the proposed algorithm show a spatial distribution of turbidity consistent with known patterns and expected values in the region, i.e., the highest turbidity values can be observed along the Barra del Indio shoal and in the southern tip of Samborombón Bay.

CONCLUSIONS

In the present study, a model to estimate turbidity based on the difference between two bands in the near infrared and short wave infrared has been developed. The use of a Rayleigh-corrected band-difference algorithm avoids the challenging task of performing the aerosol correction in highly turbid waters, like La Plata River. An overall good agreement between modelled and in situ measurements was found, especially during the cruise performed in December, while larger errors were found in March. The differences found between modelled and *in situ* values in the Samborombón Bay could be due, in part, to the fact that the atmospheric signal has not been completely removed by the band difference, i.e. the assumption of "white" aerosols might not hold. The time difference between measurements and satellite overpass, which reached up to 4 hours, did not show to be significantly correlated to the relative errors. The high spatio-temporal variability found in the sampled region is probably an important source of discrepancy. Another source of discrepancy between modelled and *in situ* values could be related to the presence of sediments with different composition and/or size distribution, and hence the turbidity-specific particle backscattering coefficient, in La Plata River compared to the regions used for the calibration of the model (24). Even though the regions used for the calibration are not geographically extensive, they show a high diversity of particle compositions and sizes which includes re-suspended mineral particles, and phytoplankton blooms (24,29). Moreover, the overall good performance of the algorithm found in

the present study suggests that there is no clear evidence yet for a regional re-calibration of the algorithm. However, more radiometric and *T/TSM in situ* measurements in highly turbid waters, like La Plata River, are clearly needed to confirm the correct calibration of the model and to validate its performance.
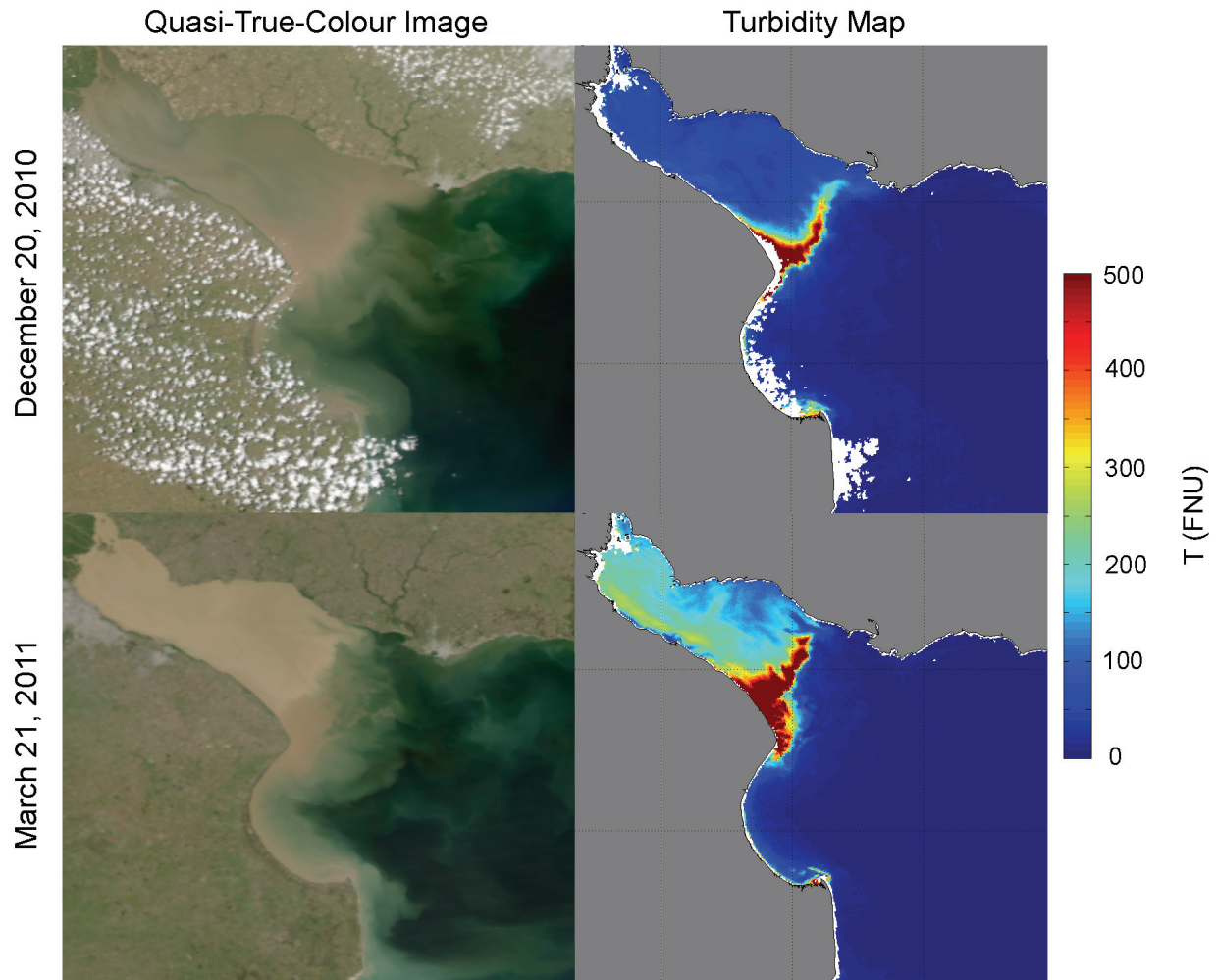
Figure 7: MODIS-Aqua Quasi-True-Colour image (left column) and Turbidity map (right column) for La Plata River Estuary on December 20, 2010 (upper panels) and March 21, 2011 (lower panels).

Finally, the calibration coefficient A_T of the model found in the present study was higher than previously found in (23) and in a recently updated version, when lower reflectance measurements were included with higher measurement uncertainties. It could also be due to the use of a fixed value for γ, which is an approximation used in this study and may not be suitable for high water reflectances. However, the spectral variation of A_T obtained using this new calibration was similar to the spectral variation of a_w, in accordance with what has been previously found (23,24).

Perspectives for improving *T* and/or *TSM* estimations in this region include the development of a better atmospheric correction algorithm which takes into account non-zero water reflectance in the SWIR bands (16,18) and the use of longer wavelength bands in new ocean colour instruments, like the 1020 nm band in the Ocean and Land Color Instrument (OLCI) on Sentinel 3 to be launched in 2013. Preliminary results showed that reflectance beyond 1000 nm is not zero in very turbid waters, like the Scheldt River, and a strong correlation between the 1020 nm band and *TSM* and turbidity was found showing its potential use for *T/TSM* retrieval (30).

REFERENCES

1   Framiñan M, M Etala, E Acha, R Guerrero, C Lasta, & O Brown, 1999. Physical characteristics and processes of the Río de la Plata Estuary. In: Estuaries of South America, Their Geomorphology and Dynamics, edited by G Perillo, M C Piccolo & M Pino-Quivira (Springer, New York), 161-191

2   Framiñan M, & O Brown, 1996. Study of the Río de la Plata turbidity front, Part 1: Spatial and temporal distribution, Continental Shelf Research, 16, 1259-1282, doi:10.1016/0278-4343(95)00071-2

3   Acha E M, H Mianzan, G Guerrero, M Favero & J Bava, 2004. Marine fronts at the continental shelves of austral South America: physical and ecological processes. Journal of Marine Systems, 44: 83-105

4   Macchi G J, E M Acha & C A Lasta, 1996. Desove y fecundidad de la corvine rubia (*Micropogonias furnieri*, Desmarest, 1826) en el estuario del Río de la Plata, Argentina. Boletín del Instituto Español de Oceanografía, 12: 99-113

5   Acha E M, H W Mianzan, C A Lasta & R A Guerrero, 1999. Estuarine spawning of the whitemouth croaker *Micropogonias furnieri* (Pisces: Sciaenidae) in the Río de la Plata, Argentina. Marine and Freshwater Research, 50: 57-65

6   Acha E M & G J Macchi, 2000. Spawning of Brazilian menhaden, Brevoortia aurea, in the Río de la Plata Estuary off Argentina and Uruguay. Fishery Bulletin, 98: 227-235

7   A Jaureguizar, R Menni, C Bremec, H Mianzan & C Lasta, 2003. Fish assemblage and environmental patterns in the Río de la Plata estuary. Estuarine Coastal and Shelf Science, 56(5-6): 921-933.

8   Militelli M I & G J Macchi, 2001. Preliminary estimate of spawning frequency and batch fecundity of Brazilian flathead, *Percophis brasiliensis*, in coastal waters off Buenos Aires Province. Scientia Marina, 65(2):169-172

9   Jaureguizar A, M Militelli & R Guerrero, 2008. Distribution of *Micopogonias furnieri* at different maturity stages along an estuarine gradient and in relation to environmental factors. Journal of the Marine Biological Association of the United Kingdom, 88(1):175-181

10 Lasta C A, 1995. La Bahía Samborombón: zona de desove y crı´a de peces. PhD thesis, National University of La Plata, Argentina

11 Canevari P, D E Blanco & E H Bucher, 1999. Los Beneficios de los Humedales de la Argentina. Amenazas y Propuestas de Soluciones. Wetlands International (Buenos Aires, Argentina) 64pp.

12 Chauhan O S, A S Rajawat, Y Pradhan, J Suneethi & S R Nayak, 2005. Weekly observations on dispersal and sink pathways of the terrigenous flux of the Ganga–Brahmaputra in the Bay of Bengal during NE monsoon. Deep-Sea Research II, 52: 2018-2030

13   Bignami F, R Sciarra, S Carniel & R Santoleri, 2006. Variability of Adriatic Sea coastal turbid waters from SeaWiFS imagery. <u>Journal of Geophysical Research</u>, 112,C03S10, doi:10.1029/2006JC003518

14   Chen Z, Ch Hu & F Müller-Karger, 2007. Monitoring turbidity in Tampa Bay using MODIS/Aqua 250-m imagery. <u>Remote Sensing of Environment</u>, 109: 207-220

15   Moore G F, J Aiken & S J Lavender, 1999. The atmospheric correction of water colour and the quantitative retrieval of suspended particulate matter in Case II waters: application to MERIS. <u>International Journal of Remote Sensing</u>, 20(9): 1713-1734

16   Wang M & W Shi, 2007. The NIR-SWIR combined atmospheric correction approach for MODIS ocean color data processing. <u>Optics Express</u>, 15: 15722-15733

17   Ruddick K G, V De Cauwer, Y Park & G Moore, 2006. Seaborne measurements of near infra-red water-leaving reflectance - the similarity spectrum for turbid waters. <u>Limnology and Oceanography</u>, 51(2): 1167-1179

18   Shi W & M Wang, 2009. An assessment of the ocean black pixel assumption for the MODIS SWIR bands. <u>Remote Sensing of Environment</u>, 113: 1587-1597

19   Wang M, S Son, & W Shi, 2009. Evaluation of MODIS SWIR and NIR-SWIR atmospheric correction algorithms using SeaBASS data. <u>Remote Sensing of Environment</u>, 113: 635-644

20   Doron M, S Bélanger, D Doxaran & M Babin, 2011. Spectral variations in the near-infrared ocean reflectance. <u>Remote Sensing of Environment</u>, 115: 1617-1631

21   Bava, J, 2004. <u>Methodologies for processing NOAA-AVHRR images and their use in oceano-graphic and biological-fishing applications in the Southwestern Atlantic Ocean</u>. Ph.D. dissertation, University of Buenos Aires, Argentina. 213 pp.

22   International Organization for Standardization (ISO), 1999. Water quality - Determination of turbidity. ISO 7027

23   Nechad B, K G Ruddick & G Neukermans, 2009. Calibration and validation of a generic multisensor algorithm for mapping of turbidity in coastal waters. In: <u>SPIE, Remote Sensing of the Ocean, Sea Ice, and Large Water Regions</u>, edited by Ch R Bostater Jr., S P Mertikas, X Neyt, M Velez-Reyes (Berlin, Germany) Vol. 7473, 74730H

24   Nechad B, K G Ruddick & Y Park, 2010. Calibration and validation of a generic multisensor algorithm for mapping of total suspended matter in turbid waters. <u>Remote Sensing of the Environment</u>, 114: 854-866

25   Morel A & L Prieur, 1977. Analysis of variations in ocean color. <u>Limnology and Oceanography</u>, 22: 709-722

26   Kou L, D Labrie & P Chylek, 1993. Refractive indices of water and ice in the 0.65-2.5 µm spectral range. <u>Applied Optics</u>, 32: 3531-3540

27   Doxaran D, M Babin & E Leymarie, 2007. Near-infrared light scattering by particles in coastal waters. <u>Optics Express</u>, 15: 12834−12849

28   Ruddick K G & G Lacroix, 2006. Hydrodynamics and meteorology of the Belgian Coastal Zone. In: <u>Current Status of Eutrophication in the Belgian Coastal Zone</u>, edited by V Rousseau, Ch Lancelot & D Cox (Presses Universitaires de Bruxelles, Belgium) 1-15

29   Sterckx S, E Knaeps, M Bollen, K Trouw & R Houthuys, 2007. Retrieval of suspended sediment from advanced hyperspectral sensor data in the Scheldt Estuary at different stages in the Tidal Cycle. <u>Marine Geodesy</u>, 30: 97-108

30   Knaeps E, D Raymaekers, S Sterckx, K Ruddick & A I Dogliotti. In-situ evidence of non-zero reflectance in the OLCI 1020nm band for a turbid estuary. <u>Remote Sensing of Environment</u>, Sentinel special issue, accepted

APPENDIX A

Analytical Solution of the quadratic equation of the Turbidity model

The model (equation 2) can be written as a quadratic equation of the form:

$$aT^2 + bT + c = 0 \qquad\qquad (A.1)$$

Where

$$a = \frac{\Delta\rho_w^{1,2}}{C_1 C_2} + \frac{1}{C_1} - \frac{1}{C_2}$$

$$b = \Delta\rho_w^{1,2}\left(\frac{A_{T2}}{C_1} + \frac{A_{T1}}{C_2}\right) + A_{T1} - A_{T2} \qquad\qquad (A.2)$$

$$c = \Delta\rho_w^{1,2} A_{T1} A_{T2}$$

which can be solved simply to give:

$$T = \frac{-b - \sqrt{b^2 - 4ac}}{2a} \qquad\qquad (A.3)$$

taking the smaller of the two roots to this quadratic equation.